

Solution versus Solid-State Structure of Ytterbium Heterobimetallic Catalysts

Lorenzo Di Bari,[†] Moreno Lelli,^{†,‡} Guido Pintacuda,^{||} Gennaro Pescitelli,[†]
Fabio Marchetti,[§] and Piero Salvadori^{†,*}

Contribution from the ICCOM-CNR, Sez. di Pisa, Dipartimento di Chimica e Chimica Industriale, Università di Pisa, Via Risorgimento 35, I-56126 Pisa, Italy, Scuola Normale Superiore, Piazza dei Cavalieri 7, I-56126 Pisa, Italy, and Dipartimento di Chimica e Chimica Industriale, Università di Pisa, Via Risorgimento 35, I-56126 Pisa, Italy

Received December 16, 2002; E-mail: psalva@dcci.unipi.it

Abstract: The solution structures of the ytterbium heterobimetallic complexes $\text{Na}_3[\text{Yb}((S)\text{-BINOL})_3]$ (**1**), $\text{K}_3[\text{Yb}((S)\text{-BINOL})_3]$ (**2**), and $\text{Li}_3[\text{Yb}((S)\text{-BINOL})_3]$ (**3**), belonging to a family of well-known enantioselective catalysts, are studied by means of NMR and circular dichroism (CD) in the UV and near-IR regions. The experimental NMR paramagnetic shifts were employed to obtain a refined solution structure of **1**. NMR analysis demonstrated that **1**, **2**, and **3** have the same solution geometry but different magnetic susceptibility anisotropy \mathcal{O} factors. By comparing XRD and NMR structures of **1**, we demonstrate that, upon dissolution, this complex experiences a rearrangement from the crystalline C_3 symmetry into the solution D_3 symmetry. Remarkably, Yb is not bound to water in solution, and Ln–BINOL bonds are labile as demonstrated through EXSY. NIR–CD is confirmed especially sensitive to changes in the ytterbium coordination sphere.

Introduction

Heterobimetallic lanthanoid catalysts are a family of complexes of general formula $\text{M}_3[\text{Ln}(\text{BINOL})_3]$ (where Ln = rare earth metal, M = Li, Na, K, and BINOL is enantiopure 1,1'-bis(2-naphthol)) introduced first by Shibasaki et al. in 1992 as stereoselective catalysts for the nitroaldolic reaction.¹ Subsequently, these systems provided excellent results in many other stereoselective reactions, such as aldol-type condensations, the Michael reaction, imines and aldehydes hydrophosphonylation, the Diels–Alder reaction, the addition of alkyllithium reagents to aldehydes, just to quote a few examples.² The interest in these systems is enhanced by the relative ease of preparation. The wide scope of these catalysts is partially explained by the smooth modulation of the steric and electronic properties which can be achieved by changing the lanthanide and the alkaline ions. To rationalize the reaction mechanisms, parallel and independent studies have been conducted by Shibasaki³ and Aspinall⁴ on the crystal structures of many derivatives, while a clear picture

of the solution structure and dynamics is still missing.⁵ We undertook a detailed analysis of NMR, NIR–CD and UV–CD data of $\text{Na}_3[\text{Yb}((S)\text{-BINOL})_3]$ (**1**) and $\text{K}_3[\text{Yb}((S)\text{-BINOL})_3]$ (**2**) and reexamined the case of $\text{Li}_3[\text{Yb}((S)\text{-BINOL})_3]$ (**3**).^{4a} For a correct reference, we also prepared and studied the Lu analogue $\text{Na}_3[\text{Lu}((S)\text{-BINOL})_3]$ (**4**). The NMR spectra of the three complexes **1–3** are compatible with the same solution structure, with labile Yb–BINOL bonds. We primarily investigated the role of water and the alkali cation and demonstrated that the axial site is not available to binding and that significant charge distribution changes are observed upon shifting from Li^+ to K^+ .

Results and Discussion

Crystallographic Structure of $\text{Na}_3[\text{Yb}((S)\text{-BINOL})_3]$ ·6THF. The complexes $\text{Na}_3[\text{Yb}((S)\text{-BINOL})_3]$ (**1**), $\text{K}_3[\text{Yb}((S)\text{-BINOL})_3]$ (**2**), and $\text{Na}_3[\text{Lu}((S)\text{-BINOL})_3]$ (**4**) were prepared in the presence of 1 equiv of H_2O , according to the procedures described in the Experimental Section. The crystalline solid obtained for **1** was subjected to X-ray diffraction (XRD) analysis, which led to the same structure of the analogous complex prepared by Aspinall in anhydrous conditions.⁴ Hence, ytterbium is only hexacoordinated (Chart 1), although water is available for axial binding. Indeed, a variation of coordination number (CN) is observed along the lanthanide series, passing from CN = 7 for elements La–Eu to CN = 6 for Eu–Yb; Eu yields both capped and noncapped coordination polyhedra.⁴

[†] ICCOM-CNR, Sez. di Pisa, Dipartimento di Chimica e Chimica Industriale, Università di Pisa.

[‡] Scuola Normale Superiore.

[§] Dipartimento di Chimica e Chimica Industriale, Università di Pisa.

^{||} Current address: Karolinska Institute, Department of Medical Biochemistry and Biophysics, Scheele Laboratory A1-4, Tomtebodavägen 6, S-171 77 Stockholm, Sweden.

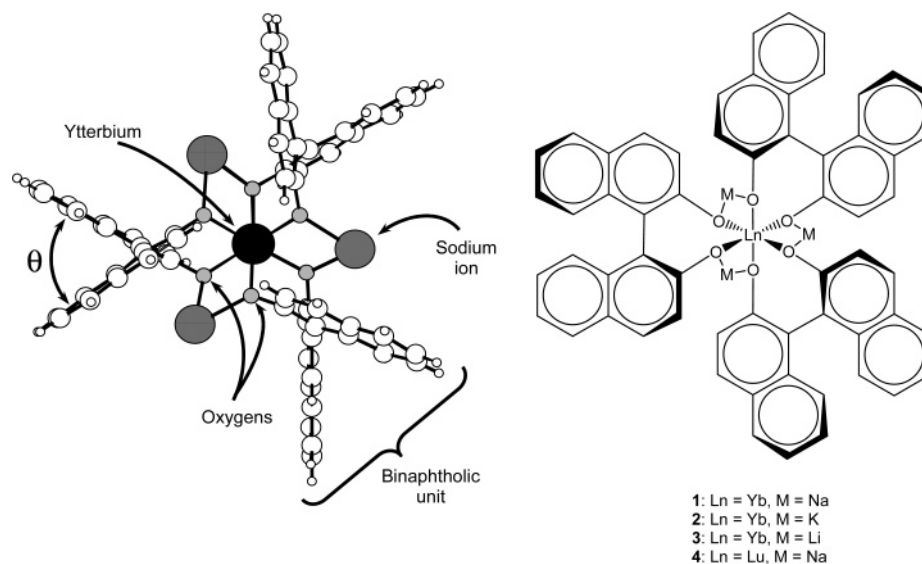
(1) Sasai, H.; Suzuki, T.; Arai, S.; Arai, T.; Shibasaki, M. *J. Am. Chem. Soc.* **1992**, *114*, 4418–4420.

(2) (a) Kobayashi, S. *Lanthanides: Chemistry and Use in Organic Synthesis, Topics in Organometallic Chemistry*; Springer-Verlag: Berlin, 1999. (b) Shibasaki, M.; Yoshikawa, N. *Chem. Rev.* **2002**, *102*, 2187–2209. (c) Aspinall, H. C.; Dwyer, J. L. M.; Greeves, N.; Steiner, A. *Organometallics* **1999**, *18*, 1366–1368.

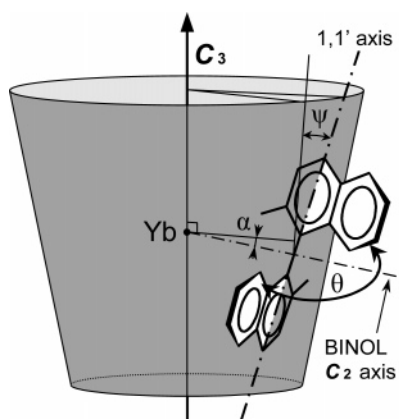
(3) Sasai, H.; Suzuki, T.; Itoh, N.; Tanaka, K.; Date, T.; Okamura, K.; Shibasaki, M. *J. Am. Chem. Soc.* **1993**, *115*, 10372–10373.

(4) (a) Aspinall, H. C.; Bickley, J. F.; Dwyer, J. L. M.; Greeves, N.; Kelly, R. V.; Steiner, A. *Organometallics* **2000**, *19*, 5416–5423. (b) Aspinall, H. C. *Chem. Rev.* **2002**, *102*, 1807–1850.

(5) In ref 4, Aspinall et al. made a preliminary analysis which will be discussed in the following.

Chart 1. Representation of the Solid-State Structure of **1**^a

^a The THF molecules coordinating each sodium atom are omitted; θ is the *intra*binaphtholic dihedral angle.

Chart 2. Definition of Conformational Parameters for Compound **1**

Ytterbium is surrounded by three symmetrically arranged binaphtholic units, having the internaphthyl $1,1'$ axis aligned *almost* parallel to the C_3 axis of the complex and the Na^+ bridging two oxygens belonging to distinct BINOLs. The coordination polyhedron is a distorted octahedron, axially compressed into a trigonal antiprism. The octahedral coordination with bidentate ligands gives rise to a Λ/Δ chirality which, in the presence of the BINOL stereogenic axis, may lead to diastereomeric structures; using (*S*)-BINOL as the ligand, only the Λ stereoisomer was found in the crystallographic structure. The Yb–O distances (2.203(8) and 2.230(8) Å) are smaller than those for early lanthanides (2.365(7) and 2.386(7) Å for Pr),³ according to the lanthanide contraction.⁶ The two different Yb–O distances found for each ligand indicate that the two naphtholic moieties of each BINOL are not equivalent. The same nonequivalence is also observed in the structures of the early lanthanide/sodium complexes, whose symmetry is not higher than C_3 ;^{3,4} however, the latter compounds are axially coordinated by water. Complex **1** has a “conical” geometry (Chart 2), which can be quantitatively described through the angle α between the local BINOL C_2 axis and the complex C_3 axis (for

simplicity, we consider only the amount exceeding 90° , as depicted in Chart 2).

The other relevant conformational parameters are the angles ψ and θ (Chart 2 and Table 3): ψ is the dihedral between the C_3 axis, the BINOL C_2 axis, and the *inter*-binaphthyl $1,1'$ axis, and θ is the dihedral between the naphthalene planes in BINOL.⁷

Solution Structure Determination through Paramagnetic NMR Analysis. The NMR spectra of complexes **1**, **2**, and **3**⁸ are dominated by the paramagnetic shift due to the unpaired electron in the *f* shell of ytterbium, as can be appreciated by comparing their resonances with those of the diamagnetic lutetium analogue **4** (Table 1).

Only one set of resonances is observed for the naphthalene nuclei, in agreement with what was already reported for $\text{K}_3[\text{Yb}(\text{BINOL})_3]$ ⁹ and for $\text{Na}_3[\text{Yb}(\text{BINOL})_3]$ and $\text{Li}_3[\text{Yb}(\text{BINOL})_3]$ *in strictly anhydrous conditions*;⁴ this indicates that the *effective* symmetry in solution is D_3 . ¹H NMR spectra show narrow line widths (see following discussion), which allowed for the resolution of proton–proton couplings and the spectral assignment of **1** on the basis of simple homonuclear decoupling experiments.¹⁰ The spectral width progressively reduces, passing from 105 ppm for **3**⁴ to 50 ppm in the case of **1** and 20 ppm for **2**.

The paramagnetic contribution (δ^{par}) to the observed shift (δ^{obs}) can be isolated by subtraction of the appropriate diamagnetic reference δ^{diam} . The term δ^{par} is the sum of two contributions, namely the contact (δ^{cont}) and pseudocontact (δ^{pc}) terms¹¹

$$\delta^{\text{par}} = \delta^{\text{obs}} - \delta^{\text{diam}}$$

$$\delta^{\text{par}} = \delta^{\text{cont}} + \delta^{\text{pc}} \quad (1)$$

The former is due to the magnetic interaction with the unpaired

(7) The angle θ is defined as the average of $2-1-1'-2'$ and $9-1-1'-9'$ dihedrals.

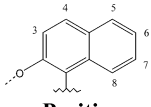
(8) NMR data of $\text{Li}_3[\text{Yb}(\text{S}-\text{BINOL})_3]$ **3** taken from ref 4a.

(9) Gröger, H.; Saida, Y.; Sasai, H.; Yamaguchi, K.; Martens, J.; Shibasaki, M. *J. Am. Chem. Soc.* **1998**, *120*, 3089–3103.

(10) ¹³C NMR spectra were assigned by a two-dimensional HETCOR experiment.

(11) Bertini, I.; Luchinat, C. *Coord. Chem. Rev.* **1996**, *150*.

(6) Quadrelli, E. A. *Inorg. Chem.* **2002**, *41*, 167–169 and references therein.

Table 1. ^1H and ^{13}C NMR Shifts for Complexes **1**, **2**, and **4** and ^1H - T_1 of Complexes **1** and **4**, in d_8 -THF


Position	^1H			^{13}C				
	δ (ppm)	T_1 (ms)	δ (ppm)	δ (ppm)	T_1 (ms)	δ (ppm)		
	YbSB ^a	YbPB ^b	LuSB ^c	YbSB	LuSB	YbSB	YbPB	LuSB
3	43.7	20.5	7.4	16	1140	149.4	132.0	127.1
4	14.5	10.1	7.6	137	827	132.7	129.0	128.3
5	7.4	7.5	7.5	386	846	125.1	126.5	128.3
6	4.5	5.7	6.8	620	928	118.2	119.6	120.2
7	3.2	5.4	6.8	480	935	119.0	122.1	124.7
8	-2.3	3.0	6.7	133	1039	117.2	121.8	125.9

^a YbSB = $\text{Na}_3[\text{Yb}(\text{S})\text{-BINOL}]_3$ (**1**). ^b YbPB = $\text{K}_3[\text{Yb}(\text{S})\text{-BINOL}]_3$ (**2**). ^c LuSB = $\text{Na}_3[\text{Lu}(\text{S})\text{-BINOL}]_3$ (**4**).

electron when it is located on the observed nucleus (Fermi or contact interaction). The latter term, in the case of an axially symmetrical complex, can be written as

$$\delta^{pc} = \mathcal{D} \frac{(3 \cos^2 \Omega - 1)}{r^3} \quad (2)$$

where \mathcal{D} is the axial magnetic susceptibility anisotropy factor, r is the distance between the observed nucleus and the paramagnetic center (Yb), and Ω is its azimuthal angle with respect to the C_3 axis. Thus, the dependence of δ^{pc} on r and Ω provides a first set of parameters for the structural analysis.

Nuclear relaxation is also affected by the paramagnetic interaction:¹¹ the contribution to longitudinal and transverse relaxation rates, ρ_1^{par} and ρ_2^{par} , respectively, in the absence of chemical exchange and neglecting outer sphere relaxation, can be written as the sum of two terms related to dipolar and Curie relaxation¹²

$$\rho_1^{par} = \frac{1}{T_1^{obs}} - \frac{1}{T_1^{diam}} = \rho_1^{dip} + \rho_1^{Curie} \quad (3)$$

where T_1^{diam} is the longitudinal relaxation time for an isostructural diamagnetic reference.

Both ρ_1^{par} and ρ_2^{par} are proportional to r^{-6} through the spectral densities J_1^{dip} and J_1^{Curie} , containing the electronic (τ_e) and rotational (τ_r) correlation times, respectively.

$$\rho_1^{Curie} = \frac{J_1^{Curie}}{r^6}$$

$$\rho_1^{dip} = \frac{J_1^{dip}}{r^6} \quad (4)$$

In a situation reminiscent of extreme narrowing ($(2\pi\nu\tau_e)^2$, $(2\pi\nu\tau_r)^2$, $(2\pi\nu_e\tau_e)^2 \ll 1$, with ν the Larmor frequency of the observed nucleus and ν_e the electron Larmor frequency), J_1^{dip} and J_1^{Curie} become directly proportional to their respective correlation times, and ρ_1^{par} and ρ_2^{par} can be rewritten invoking two phenomenological correlation times $\tau_{c(1)}$ and $\tau_{c(2)}$, which contain a linear combination of τ_e and τ_r .

(12) The contact contribution is usually considered negligible, ref 11.

$$\rho_1^{par} = \frac{(k_1^{Curie}\tau_r + k_1^{dip}\tau_e)}{r^6} = \frac{K}{r^6}\tau_{c(1)}$$

$$\rho_2^{par} = \frac{(k_2^{Curie}\tau_r + k_2^{dip}\tau_e)}{r^6} = \frac{K}{r^6}\tau_{c(2)}$$

$$\tau_{c(1)} = (\tau_e + A_1\tau_r)$$

$$\tau_{c(2)} = (\tau_e + A_2\tau_r)$$

$$K = \frac{4}{3} \left(\frac{\mu_0}{4\pi} \right)^2 \gamma_I^2 g^2 \mu_B^2 [J(J+1)]$$

$$A_1 = \frac{6}{7}A_2 = \frac{9}{10} \frac{B_0^2 g^2 \mu_B^2 [J(J+1)]}{(3kT)^2} \quad (5)$$

where μ_0 , μ_B , γ_I , B_0 , k , and T are, respectively, the vacuum magnetic permeability, the Bohr magneton, the magnetogyric ratio, the magnetic field, the Boltzmann constant, and the absolute temperature; for Yb^{3+} , $J = 7/2$ and $g = 8/7$. It must be noticed that $\rho_1^{par} \neq \rho_2^{par}$, owing to the Curie term. The dependence of ρ^{par} on the Yb-nucleus distance (r) provides a second set of constraints (in addition to δ^{par}) for the geometrical analysis.

Solution Structure of $\text{Na}_3[\text{Yb}(\text{S})\text{-BINOL}]_3$ (1**).** Isolating the pseudocontact term δ^{pc} from the NMR spectra of Yb complexes was particularly easy because (a) it is generally accepted that the contact term δ^{cont} is negligible for this ion^{11,13} and (b) an excellent estimate of δ^{diam} and ρ_1^{diam} for each nucleus is provided by the isostructural lutetium system.¹⁴

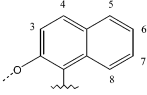
The measurement of the ρ_2 's through the line widths was plagued by the proton-proton couplings, so we considered only ρ_1^{par} values which were estimated by means of eq 3, with reference to the corresponding values for the Lu analogue **4**.

First of all, we verified whether the crystallographic structure of **1** might be an acceptable approximation for the solution structure; to this end, the experimental δ^{pc} and ρ_1^{par} values were compared with those calculated on the basis of XRD coordinates through eqs 2 and 5. The geometrical factors $(3 \cos^2 \Omega - 1)/r^3$ (GF) in eq 2 might be obtained from the XRD coordinates¹⁵ after determining the orientation of the C_3 axis; this was not easily accessible because of the symmetry-breaking distortion

(13) Di Bari, L.; Pintacuda, G.; Salvadori, P. *Eur. J. Inorg. Chem.* **2000**, 75–82.

(14) Considering the differences that exist between diamagnetic spectra reported in ref 4a, one concludes that the Lu–Na complex **4** is the diamagnetic complex more akin to **1**.

Table 2. Geometrical Factors (GF) and Distances between Yb and the Observed Nucleus ($r_{\text{Yb-X}}$) Calculated from the Paramagnetic NMR Analysis on the Symmetrized Crystal Structure (without ligand rearrangement), and Symmetric Structure (considering the ligand rearrangement) for Compound 1



Position	Symmetrized Crystal Structure ^a				Symmetric Structure ^b	
	GF ($\times 10^3$) (\AA^{-3})		$r_{\text{Yb-X}}$ (\AA)		GF ($\times 10^3$) (\AA^{-3})	$r_{\text{Yb-X}}$ (\AA)
C3	14.2	4.74	4.0	4.1	12.0	3.9
C4	5.10	0.707	5.1	5.2	3.05	5.0
C5	-0.00527	-1.48	6.7	7.0	-1.36	6.7
C6	-0.891	-1.68	7.6	7.7	-1.89	7.4
C7	-1.98	-2.39	7.2	7.3	-2.89	6.9
C8	-4.00	-4.39	6.0	6.0	-5.37	5.7
H3	22.0	13.7	4.0	4.1	20.5	4.0
H4	5.23	2.08	5.8	5.9	3.71	5.7
H5	0.738	-0.617	7.5	7.6	-0.397	7.3
H6	-0.554	-1.14	8.5	8.6	-1.32	8.3
H7	-1.67	-1.83	7.9	7.9	-2.27	7.6
H8	-4.52	-4.19	6.0	6.0	-5.36	5.6

^a Two different values are reported, relative to the two different sets of naphtholic units. ^b Mean values over all equivalent nuclei.

present in the molecule. On the other hand, the C_3 axis coincides with the principal axis of the magnetic susceptibility tensor, so it was indirectly obtained as a parameter by fitting the experimental data (δ^{pc} , T_1) through the previously mentioned eqs 2 and 5. Four parameters were optimized: the orientation of the C_3 axis (2 degrees of freedom), the anisotropy factor \mathcal{D} (1 degree of freedom), and the phenomenological constant $\tau_{c(1)}$ (1 degree of freedom). We used twelve pseudocontact shifts (for protons and protonated carbons) and six values of T_1 (only for protons) to solve the problem.¹⁶

A computer program (called PERSEUS)¹⁷ fitted the unknown parameters until the function F reached a local minimum:

$$F = \frac{\sum_{i=1}^s A_i (\delta_i^{pc(\text{calc})} - \delta_i^{pc(\text{exper})})^2}{\sum_{i=1}^s (\delta_i^{pc(\text{exper})})^2} + \frac{\sum_{m=1}^t B_m (\rho_m^{\text{par}(\text{calc})} - \rho_m^{\text{par}(\text{exper})})^2}{\sum_{m=1}^t (\rho_m^{\text{par}(\text{exper})})^2} \quad (6)$$

We found it adequate to keep all the weights A_i and B_m equal to unity. Calculated geometrical factors (GF) are reported in

(15) A referee drew our attention to the fact that using "X-ray coordinates during the NMR structure elucidation an inaccuracy is introduced, because the C-H bonds as determined by X-ray are too short, since the location of the highest electron density is observed". This is indeed correct in the present case: we found $\langle d_{\text{C-H}} \rangle = 0.93 \text{ \AA}$, but correcting the coordinate file by imposing $d_{\text{C-H}} = 1.08 \text{ \AA}$ had no influence on the NMR data analysis through PERSEUS. One must take into account that the accuracy of paramagnetic NMR is limited by several factors (e.g., line width, bulk paramagnetism, neglect of contact terms).

Table 3. Fitting Parameters and Mean Values for the Complex Conformations Derived from the NMR Analysis on the Symmetrized Crystal Structure (without Ligand Rearrangement) and Symmetric Structure (Considering the Ligand Rearrangement) for Compound 1

Fitting and Ligand Parameters ^a	Symmetrized Crystal Structure	Symmetric Structure
\mathcal{D} , ppm \AA^3	1900 \pm 60	1770 \pm 50
θ , deg	63 \pm 1	73 \pm 2
ψ , deg	11 \pm 1	19 \pm 2
α , deg	5 \pm 1	0
$\tau_{c(1)}$, ps	0.17 \pm 0.01	0.156 \pm 0.004
$R(\delta^{pc})$, ^b %	13	5.5
$R(\rho^{\text{par}})$, ^b %	1.8	3.7

^a See Chart 2 for a definition of α , ψ , and θ . ^b Agreement factors defined as $R(\delta) = [(\sum_i (\delta_i^{pc(\text{calc})}) - \delta_i^{pc(\text{exper})})^2 / \sum_i (\delta_i^{pc(\text{exper})})^2]^{1/2}$ and $R(\rho) = [(\sum_i (\rho_i^{\text{par}(\text{calc})}) - \rho_i^{\text{par}(\text{exper})})^2 / \sum_i (\rho_i^{\text{par}(\text{exper})})^2]^{1/2}$, where $\langle \delta_i^{pc(\text{calc})} \rangle$ and $\langle \rho_i^{\text{par}(\text{calc})} \rangle$ are the mean values calculated over all the equivalent nuclei; the sums under the square roots run over twelve δ^{pc} and six ρ^{par} .

Table 2 (Symmetrized Crystal Structure column). The optimized parameters \mathcal{D} and $\tau_{c(1)}$, the ligand conformations, and the agreement factor between experimental and calculated values are reported in Table 3 (Symmetrized Crystal Structure column). The agreement factor of 13% is only fair, in comparison with other structural determinations involving Yb as the paramagnetic center.^{13,18}

The conical distortion of the complex (angle α , Chart 2) differentiates the dipolar interaction for the two naphtholic moieties, so that very large differences in δ^{pc} were calculated for corresponding nuclei (e.g., 15 ppm for H3 and H3'), although only six proton resonances were observed in solution. The apparently higher symmetry of the solution structure can be explained only in two ways: (a) In solution, two forms with

(16) The paramagnetic relaxation rates of ^{13}C were less accurate and did not improve the quality of the fitting.

(17) Di Bari, L.; Pintacuda, G.; Ripoli, S.; Salvadori, P. *Magn. Reson. Chem.* **2002**, *40*, 396–405.

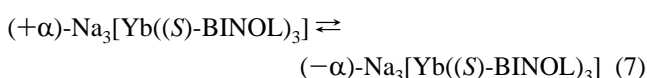
(18) Brittain, H. G.; Desreux, J. F. *Inorg. Chem.* **1984**, *23*, 4459–4466.

Table 4. Experimental and Calculated ^1H Line Widths for $\text{Na}_3[\text{Yb}((S)\text{-BINOL})_3]$ (**1**)

Protons	$r_{\text{Yb-H}}$ (Å) ^a	Experimental linewidth (Hz) ^b	Calculated linewidth (Hz)
H3	4.1	28.9	21.9
H4	5.9	8.9	3.3
H5	7.5	3.6	1.5
H6	8.6	< 4	1.2
H7	8.0	< 4	1.3
H8	6.0	< 6	3.1

^a Mean value of the Yb–H distances for equivalent protons in the crystal structure. ^b The data relative to protons 6–8 are inaccurate owing to partially unresolved multiplets; upper limits are shown.

opposite conicity ($\pm\alpha$) are in fast exchange on the NMR time scale (*dynamic symmetry*)



(b) Upon dissolution, the complex undergoes a rearrangement leading to a D_3 structure (*static symmetry*).

To check the former hypothesis, we assessed limiting values for the kinetic process in eq 7, by means of a detailed analysis of the line broadening in the ^1H NMR spectra. The observed line widths are generally narrow (Table 4); for a small molecule in fast motion limit, ρ_2 can be roughly estimated on the basis of eq 5.¹⁹ By using the crystallographic Yb–H distance and the correlation times $\tau_e = 0.1$ ps²⁰ and $\tau_r = 130$ ps,²¹ a reasonable agreement was found between calculated and experimental data for **1**, indicating that the paramagnetic line broadening accounts for most of the line width increase.

Nevertheless, we can set a lower limit to the kinetic constant of the equilibrium in eq 7: we can assume the calculated line widths of Table 4 as corresponding to the absence of exchange and that any exceeding broadening in the experimental spectrum arises from the dynamic process through the relation¹¹

$$\rho_2^{obs} - \rho_2 = k_{exch} - \sqrt{k_{exch}^2 - (\pi\Delta\nu_{+\alpha/-\alpha})^2} \quad (8)$$

where ρ_2^{obs} is related to the observed line width, $\Delta\nu_{+\alpha/-\alpha}$ is the difference between the calculated resonance frequencies (in Hz) for a pair of corresponding protons on one BINOL (e.g., H3 and H3'). As it can be seen, $\Delta\nu_{+\alpha/-\alpha}$ is largest for the proton pair H3–H3' (about 4700 Hz), which leads to $k_{exch} \geq 10^7$ s⁻¹.

Even at low temperature (–100 °C), the lines appeared comparatively narrow and no decoalescence occurred, despite the expected reduced exchange rate (according to the Eyring law) and the enhanced shift brought about by the temperature dependence of \mathcal{D} . For all these reasons, the *dynamic symmetrization* is reasonably excluded and a structural rearrangement must occur upon dissolution.

To get insight into the solution structure, we started from the crystal geometry, varying systematically the relevant degrees

of freedom until the best agreement between calculated and experimental NMR data was reached. Since we did not expect any substantial modification of the naphtholic units' geometries, we only varied the ytterbium coordinates (3 degrees of freedom) and the torsion angles θ (in view of the flexibility of 1,1'-binaphthyl derivatives)^{32a} (1 degree of freedom), as well as the orientation of the C_3 axis and the values of \mathcal{D} and $\tau_{c(l)}$; this led to 8 parameters overall.

As an experimental constraint, in addition to the NMR data (12 δ^{pc} and 6 $^1\text{H-T}_1$), a further term was introduced into eq 6 to keep the Yb–O distance close to a standard bond length ($\langle r_{\text{Yb-O}} \rangle = 2.2$ Å):

$$F = \frac{\sum_{i=1}^s A_i (\delta_i^{pc(\text{calc})} - \delta_i^{pc(\text{exper})})^2}{\sum_{i=1}^s (\delta_i^{pc(\text{exper})})^2} + \frac{\sum_{j=1}^r B_j (\rho_j^{par(\text{calc})} - \rho_j^{par(\text{exper})})^2}{\sum_{j=1}^r (\rho_j^{par(\text{exper})})^2} + \frac{\sum_{k=1}^t C_k (r_{k(\text{Yb-O})} - \langle r_{\text{Yb-O}} \rangle)^2}{t \langle r_{\text{Yb-O}} \rangle^2} \quad (9)$$

where the third sum goes over the t oxygen atoms, and weights $A_i = B_j = 1$ and $C_k = 100$ were used. The results of this optimization are reported in Tables 2 and 3 (Solution Structure column); Figure 1 displays calculated and experimental ^1H and ^{13}C NMR spectra. The intensity variation apparent in the plots is a consequence of the different line broadening due to Curie and dipolar relaxation.

It is clear that the structure obtained fits very well all the experimental NMR data: the agreement factor R (Table 3) for the optimized solution structure is markedly smaller than that for the crystal structure (obtained averaging the $\delta^{pc(\text{calc})}$ of all the equivalent nuclei). The optimized solution structure shows a marked difference with respect to the crystal one, especially for the conformational angles θ and ψ ; this confirms that a thorough rearrangement takes place upon dissolution.

It must be observed that the water resonance lies at 2.40 ppm, which is exactly the position of free water in d_8 -THF; the absence of a peak of coordinated water indicates that, as in the solid state, Yb is only six-coordinated.

Solution Structure of $\text{K}_3[\text{Yb}((S)\text{-BINOL})_3]$ (2**) and $\text{Li}_3[\text{Yb}((S)\text{-BINOL})_3]$ (**3**).** Both ^1H NMR spectra of **2** and **3** show only six resonances,²² in analogy to **1**; however, the signals span a very different spectral window (Table 1). Again in analogy to **1**, the position of the free water signal and the absence of a peak of bound water indicate that, also in the complex **2**, Yb is not coordinated to water in solution.

It is easily seen that the pseudocontact shifts for all the three paramagnetic complexes are *exactly* proportional, which implies either that they have the same solution structure or that different structures would lead to *accidentally* equal (within a certain tolerance) sets of geometrical factors. Although the second

(19) In eq 3, a diamagnetic contribution of 1 Hz to the line widths was used, thus $1/T_2^{diam} = 3$ s⁻¹.

(20) Alsaadi, B. M.; Rossotti, F. J. C.; Williams, R. J. P. *J. Chem. Soc., Dalton Trans.* **1980**, 2151–2154.

(21) Determined by the $^{13}\text{C-T}_1$ of the diamagnetic complex **4**.

(22) Ten resonances are found in the ^{13}C NMR spectra.

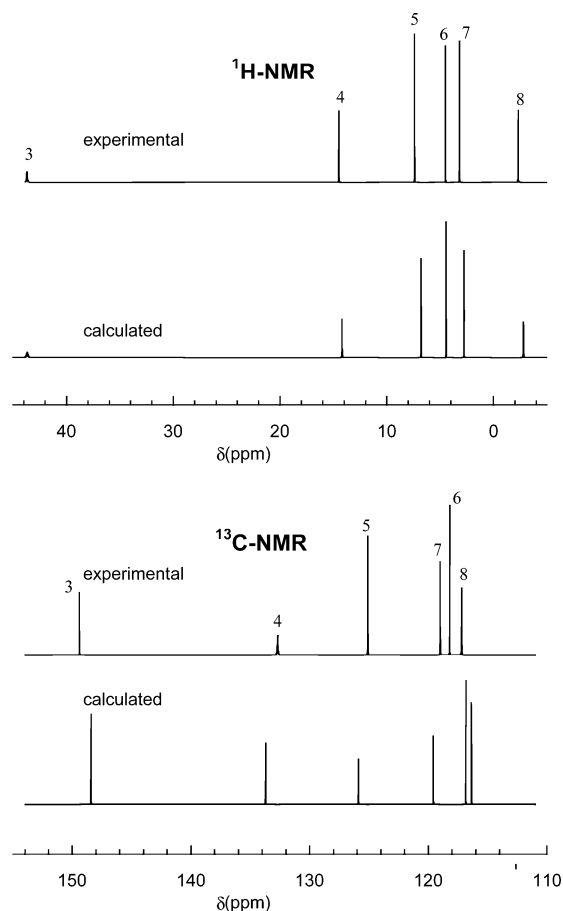


Figure 1. Reconstructed experimental and calculated ^1H and ^{13}C NMR spectra of **1**.

hypothesis was demonstrated true for azamacrocyclic ligands such as DOTMA and DOTA,¹³ we deemed this event unrealistic in the present case²³ and used the geometrical factors previously optimized to fit the δ^{pc} 's of **2** and **3** (Figure 2).

One must conclude that **1**, **2**, and **3** have the same structure and that the geometry outlined in the previous paragraph is also effective for the lithium and potassium complexes; changing the alkaline cation brings about a large change in the susceptibility anisotropy factor \mathcal{D} (1770 for **1**, 645 for **2**, and 4040 ppm \AA^3 for **3**).

The direct proportionality of the paramagnetic shifts indicates that, as generally accepted, the contact term is negligible with respect to the dipolar one, even in a complex such as **2** with a reduced \mathcal{D} factor. This is strictly true as far as the proton shifts are concerned; nonetheless, by plotting $^{13}\text{C}-\delta^{pc}$ instead of $^1\text{H}-\delta^{pc}$, a linear trend is still observed, with the largest deviation for the C3. This may indicate that, for this nucleus, separated by only three bonds from ytterbium, the contact contribution cannot be totally neglected.

The sensitivity of \mathcal{D} to the alkali ion cannot be attributed, as in other cases, to a different axial ligand,²⁴ because **3** was

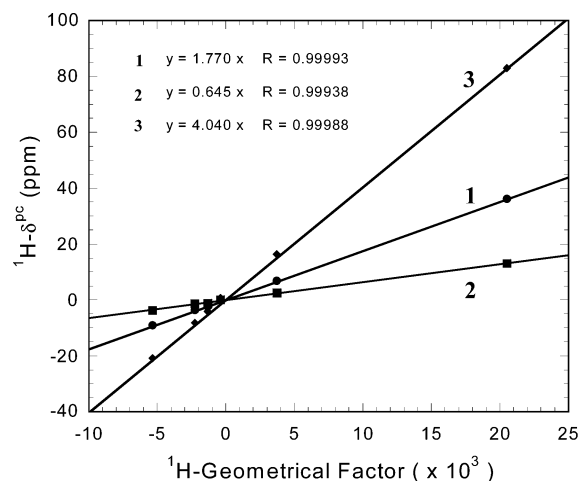


Figure 2. Relation between δ^{pc} of **1**, **2**, and **3** and the geometrical factor ($\text{GF} \times 10^3, \text{\AA}^{-3}$) calculated for the solution structure of **1**.

prepared and analyzed under strictly anhydrous conditions, and in **1** and **2** water coordination must be excluded (see *vide supra*). Thus, upon changing the alkaline ion, a charge redistribution involving the anionic oxygen atoms takes place; accordingly, a different crystal field is sensed by ytterbium in **1**, **2** and **3**, following a smooth trend with electronegativity and ionic radius.

The low coordination capability of ytterbium in these complexes (Yb is six coordinated even in the presence of free water) and their isostructurality may have important consequences for the catalytic behavior. In this regard, it is noteworthy that, by the addition of a little amount of (*S*)-BINOL to a solution of $\text{K}_3[\text{Yb}((\text{S})\text{-BINOL})_3]$,²⁵ it was shown by an EXSY experiment that there is an exchange between free and bound ligand (slow on the NMR time-scale). This demonstrated that the BINOL coordination is labile. A detailed investigation of the latter phenomenon will be the subject of a separate paper.

NIR-CD Investigation of $\text{Na}_3[\text{Yb}((\text{S})\text{-BINOL})_3]$ (1**) and $\text{K}_3[\text{Yb}((\text{S})\text{-BINOL})_3]$ (**2**).** The atomic spectrum of a free Yb^{3+} ion is characterized by one *intraconfigurational* transition ($^2F_{7/2} \rightarrow ^2F_{5/2}$)²⁶ occurring in the near-infrared (NIR) region at about 980 nm. This transition is electric-dipole forbidden and magnetic-dipole allowed ($|\Delta J| = 1$), giving comparatively high rotational strengths, which makes ytterbium(III) particularly suited for CD spectroscopy.²⁷ The ground and excited states are split by the crystal field into, respectively, four and three doubly degenerate sublevels, and their separation depends on the intensity of the crystal field due to the ligands. In complex **1**, the spectral width is about 1600 cm^{-1} , which amounts to around $10kT$ at room temperature; up to twelve transitions must be expected due to the Boltzmann populations of the upper sublevels of the ground state (*hot bands*). The NIR-CD and absorption spectra of **1** and **2** are reported in Figure 3. The spectra of **2** are very similar to those of **1**, but they span a smaller spectral width (by about 150 cm^{-1}) around the multiplet center-of-gravity at 980 nm, giving an *apparent* red shift of the most prominent transitions. Indeed, the center-of-gravity of the Yb spectrum is expected to be rather insensitive to the ligand, which,

(23) For the analysis of the pseudocontact shifts of **1** and **3**, Aspinall and co-workers (ref 4a) used the respective XRD structures, which are indeed different from each other. These authors, however, fail to observe that the symmetric XRD structure of **3** fits equally well the NMR spectra of both derivatives. The accord is less satisfactory for the artificially symmetrized structure of **1**, instead, where a nonvanishing intercept must be introduced to fit the data.

(24) Di Bari, L.; Pintacuda, G.; Salvadori, P.; Dickins, R. S.; Parker, D. *J. Am. Chem. Soc.* **2000**, *122*, 9257–9264.

(25) About 1 equiv of (*S*)-BINOL was added to a d_5 -THF solution of **2**.

(26) Richardson, F. S. *Inorg. Chem.* **1980**, *19*, 2806–2812.

(27) Di Bari, L.; Pintacuda, G.; Salvadori, P. *J. Am. Chem. Soc.* **2000**, *122*, 5557–5562.

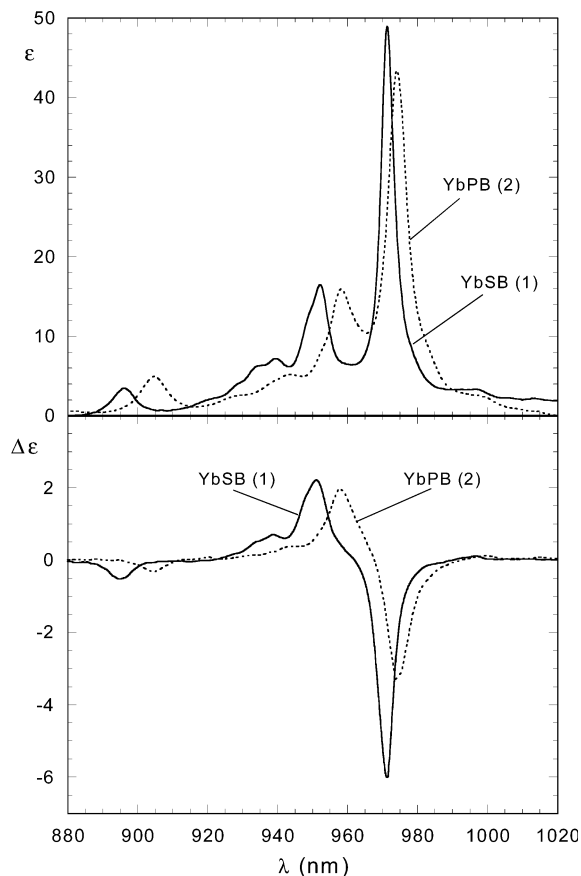


Figure 3. Absorption and NIR-CD spectra of complexes (S)-YbSB (**1**, solid line) (12.6 mM) and (S)-YbPB (**2**, dotted line) (19.4 mM) in dry THF.

on the contrary, affects the crystal field splitting. Three bands are easily recognized, appearing for **1** at 895, 951, and 971 nm; their CD intensity gives evidence of a very favorable g factor (around 0.1), as expected for transitions that are generally magnetic-dipole allowed. Because of the apparent overlap, a safe spectral assignment is difficult.

The lower energy transitions, originating from excited sublevels of the fundamental ${}^2F_{7/2}$ state, give rise to weak absorption/Cotton effects not detected in the current case.²⁷ The shrinkage of the spectra of **2** compared to **1** is thus correlated with the crystal field parameters, which are partially dependent on the alkali cation. Thus, there is a strict correlation between optical spectra and the \mathcal{D} coefficient previously determined through the analysis of the NMR spectra, as prescribed by Bleaney's theory.²⁸

The correspondence between the spectral features of compounds **1** and **2** also confirms the identical solution geometry.

Quantitative Exciton Analysis of UV-CD Spectra of $\text{Na}_3[\text{Yb}((S)\text{-BINOL})_3]$ (1**), $\text{K}_3[\text{Yb}((S)\text{-BINOL})_3]$ (**2**), and $\text{Na}_3[\text{Lu}((S)\text{-BINOL})_3]$ (**4**).** Figures 4 and 5 report the UV absorption and CD spectra of compounds **1**, **2**, and **4**. Up to 400 nm, they are entirely dominated by the $\pi\text{-}\pi^*$ transitions of the aromatic chromophore,²⁹ and the coupling with the low-energy lanthanide transitions is not appreciated, as demonstrated by the equivalence of the UV-CD spectra of ytterbium and lutetium analogues. This observation allows the interpretation of

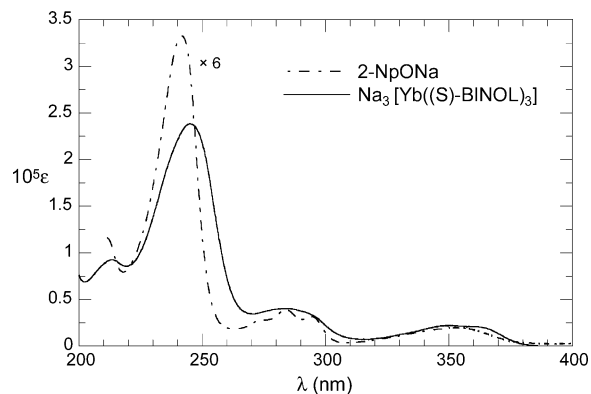


Figure 4. UV-vis spectra of $\text{Na}_3[\text{Yb}((S)\text{-BINOL})_3]$ (**1**) 0.209 mM in THF (solid line) and of 2-naphthol 1.07 mM in NaOH 0.1 M (dotted dashed line).

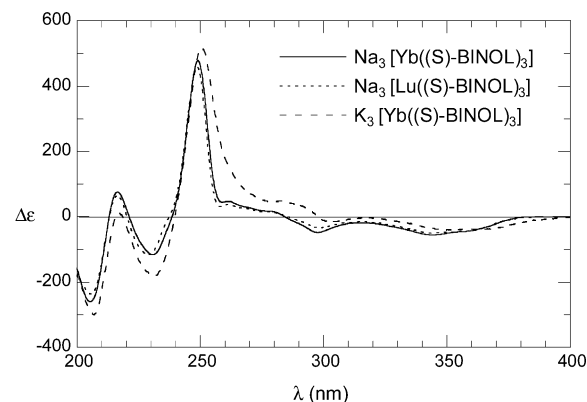


Figure 5. CD-UV spectra of $\text{Na}_3[\text{Yb}((S)\text{-BINOL})_3]$ (**1**) 0.209 mM in THF (solid line), $\text{Na}_3[\text{Lu}((S)\text{-BINOL})_3]$ (**4**) 0.161 mM in THF (dotted line), and $\text{K}_3[\text{Yb}((S)\text{-BINOL})_3]$ (**2**) 0.250 mM in THF (dashed line).

UV spectra by means of the exciton model,³⁰ in strict analogy with corresponding treatments carried out on 1,1'-binaphthyl derivatives:³¹⁻³³ in the presence of strong electric-dipole allowed transitions located on independent chromophores, the coupling between "monomer" (i.e., the naphthalene unit) transition dipoles may almost entirely account for the observed optical activity of the "aggregate".

In the present case, the very good agreement between the positions and the relative intensities of absorption bands of **1** and sodium 2-naphthoate (Figure 4) witnesses the similarity between the electronic structure of naphthyl moieties in the two compounds and justifies the use of the latter as a model monomer for the former. The apparent broadening of the most intense UV absorption in the spectrum of **1**, allied to the 1B_b transition, is a consequence to the exciton splitting.

The CD spectra of **1**, **2**, and **4** (Figure 5) appear to be superimposable; given the well-recognized enhanced sensitivity

(28) Bleaney, B. *J. Magn. Reson.* **1972**, *8*, 91-100.

(29) (a) Jaffé, H. H.; Orchin, M. *Theory and Applications of Ultraviolet Spectroscopy*; Wiley: New York, 1962. (b) Rubio, M.; Merchán, M.; Ortí, E.; Roos, B. O. *Chem. Phys.* **1994**, *179*, 395-409.

(30) (a) Harada, N.; Nakanishi, K. *Circular Dichroic Spectroscopy - Exciton Coupling in Organic Stereochemistry*; University Science Books: Mill Valley, CA, 1983. (b) Berova, N.; Nakanishi, K. In *Circular Dichroism: Principles and Applications*, 2nd ed.; Berova, N., Nakanishi, K., Woody, R. W., Eds.; Wiley-VCH: New York, 2000; Chapter 12.

(31) Mason, S. F.; Seal, R. H.; Roberts, D. R. *Tetrahedron* **1974**, *30*, 1671-1682.

(32) (a) Di Bari, L.; Pescitelli, G.; Salvadori, P. *J. Am. Chem. Soc.* **1999**, *121*, 7998-8004. (b) Di Bari, L.; Pescitelli, G.; Marchetti, F.; Salvadori, P. *J. Am. Chem. Soc.* **2000**, *122*, 6395-6398. (c) Di Bari, L.; Pescitelli, G.; Reginato, G.; Salvadori, P. *Chirality* **2001**, *13*, 548-555.

(33) (a) Rosini, C.; Rosati, I.; Spada, G. P. *Chirality* **1995**, *7*, 353-358. (b) Rosini, C.; Superchi, S.; Peerlings, H. W. I.; Meijer, E. W. *Eur. J. Org. Chem.* **2000**, 61-71. (c) Proni, G.; Spada, G. P.; Lustenberger, P.; Welti, R.; Diederich, F. *J. Org. Chem.* **2000**, *65*, 5522-5527.

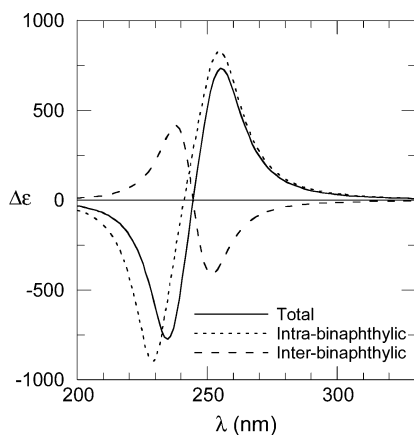


Figure 6. 1B_b CD couplet calculated, for various terms, by means of DeVoe's method for the NMR-optimized solution structure of compound **1**; see ref 37 for details.

of CD spectra to the molecular structure, this result further confirms the structural similarities between compounds **1**, **2**, and **4** in THF solution, as discussed previously. The couplet due to the 1B_b transitions is positive, as expected for the (*S*) configuration;³¹ it is also strongly nonconservative, with extrema $\Delta\epsilon_{max}$ (249 nm) = +480 and $\Delta\epsilon_{min}$ (230 nm) = -116 (for **1**) and a crossover at 242 nm. Among the factors concurring to such asymmetry is the nondegenerate coupling with high energy transitions (naphthalene 1B_a),²⁹ giving rise to the second apparent couplet with a crossover at 213 nm and the 1L_a (297 nm) and 1L_b (344 nm) transitions, both allied to negative Cotton effects.^{31–33}

Whenever the exciton mechanism of optical activity is recognized to be the dominant one, UV-CD spectra can be quantitatively predicted by means of the coupled oscillators DeVoe's method,³⁴ for which only a spectroscopic description of monomers is required.^{32,35} In the current case, however, a full interpretation of spectra is hampered by the difficulty of describing the whole electronic structure of the aromatic chromophores. In particular, the high energy 1B_a transition has been only occasionally included, with discordant results, in the plentiful work done on 2-naphthol,³⁶ and above all, no suitable treatment of 2-naphthoate appears to be available, because of the inner difficulties encountered in quantum-mechanics calculations when dealing with anions. For such reasons, we concentrated upon the 1B_b couplet, a spectral feature with a large content of structural information for 1,1'-binaphthyl derivatives.^{31,32} In particular, the wavelength splitting $\Delta\lambda_{max}$ (the wavelength difference between the two resolved couplet components with opposite sign) is in strict correlation with the dihedral angle θ defined by the two naphthalene planes.³²

Figure 6 reports calculated 1B_b couplets for **1** using the NMR-optimized solution structure;^{37,38} the different contributions from *intra*binaphthyl (that is, between directly attached naphthalenes) and *inter*binaphthyl (between not attached naphthalenes) couplings are showed. It is clear that neglecting long-range *inter*binaphthyl couplings would introduce a severe error in

the calculation. This term gives rise to a couplet with opposite sign and half the intensity of the one due to the *intra*binaphthyl term; very notably, only if the former term is included too, the wavelength splitting $\Delta\lambda_{max}$ shifts from 27 nm to the value of 20 nm which is in fine agreement with the experimental one (19 nm).³⁹

On the other hand, the couplet intensity is evidently overestimated; this discrepancy is common to all exciton-type calculations of 1,1'-binaphthyl derivatives,³² which makes any correlation based on intensity-dependent parameters less safe.^{31,33} In conclusion, UV-CD spectroscopies fully substantiate the structural assessment achieved through the NMR analysis.

Conclusions

By a careful analysis of the NMR data, the solution structures of complexes **1** and **2** were fully determined and compared with the one obtained through XRD of **1** in the solid state. Meaningful differences were found, which undoubtedly sheds new light on this notable class of molecules, especially in view of their applications as efficient catalytic precursors in many enantioselective reactions. We demonstrated that (a) a true structural rearrangement occurs upon dissolution; (b) the Ln-BINOL bond is labile; (c) the nature of alkali metal affects the charge distribution around Yb and, hence, the NMR spectra; and (d) water is not bound to the system even in the presence of as much as three equivalents of free water.

These results have important consequences in interpreting the catalysis promoted by these systems: the solid-state structures must be regarded only as a first-order approximation to the geometry of the catalytic precursor in solution; notably, when changing the alkali ion, the different behaviors have to be sought in the charge redistribution rather than in structural variations. The absence of water demonstrates that any mechanism invoking a role for the axial ligand must be rejected, at least when Ln = Yb. More likely, on account of the labile ligands, substrate binding occurs only after one BINOL unit is at least partly detached.

The three techniques (UV- and NIR-CD, paramagnetic NMR) and the data analyses employed here concur in defining a coherent stereochemical description of these systems, provid-

(34) (a) DeVoe, H. *J. Chem. Phys.* **1964**, *41*, 393–400. (b) DeVoe, H. *J. Chem. Phys.* **1965**, *43*, 3199–3208.
 (35) (a) Cech, C. L.; Hug, W.; Tinoco, I., Jr. *Biopolymers* **1976**, *15*, 131–152. (b) Rosini, C.; Zandomeneghi, M.; Salvadori, P. *Tetrahedron: Asymmetry* **1993**, *4*, 545–554.
 (36) (a) Nishimoto, K. *J. Phys. Chem.* **1963**, *67*, 1443–1446. (b) Forster, L. S.; Nishimoto, K. *J. Am. Chem. Soc.* **1965**, *87*, 1459–1463.

(37) DeVoe-type calculations were carried out with a computer routine due to Hug (ref 35a). Spectral parameters (frequency maximum, dipolar strength, and half-height width) were taken from the UV spectrum of sodium 2-naphthoate. 1B_b transition dipoles were placed in the centers of aromatic planes and oriented along the C6–C2 direction; an angle of about 15° between the 1B_b transition polarization and naphthalene long axis is found by CNDO calculations on 2-naphthoate (ref 38). See ref 32b for a discussion about the role played by transition polarizations on exciton-type calculations on 1,1'-binaphthyl derivatives.
 (38) CNDO/S-CI calculations were carried out with a CNDO/M program, according to Del Bene and Jaffé's formulation [Del Bene, J.; Jaffé, H. H. *J. Chem. Phys.* **1968**, *49*, 1221–1229], with a Mataga approximation of two-electron repulsion integrals. Up to 60 singly excited states, with maximum energy values of 7.0 eV, were included in the CI. B3LYP-DFT optimized structures (carried out with Gaussian 94, Gaussian, Inc.: Pittsburgh, PA) were used as the input geometries.
 (39) It seems that the fine agreement here found cannot be extended to a recent report concerning $\text{Na}_3[\text{Fe}((S)\text{-BINOL})_3]\cdot 3\text{Et}_2\text{O}\cdot\text{H}_2\text{O}$, a complex closely analogous to **1**, **2**, and **4**, for which a dihedral angle $\theta = 56^\circ$ is found in the solid state [Cross, R. J.; Farrugia, L. J.; McArthur, D. R.; Peacock, R. D.; Taylor, D. S. C. *Inorg. Chem.* **1999**, *38*, 5698–5702]. In the CD spectrum of this Fe complex, the 1B_b couplet is quite symmetric and seems unaffected by high-energy transitions (giving rise to weaker Cotton effects); moreover, the wavelength splitting $\Delta\lambda_{max}$ has the totally unexpected low value of 14.5 nm, and no striking structural difference is evident with respect to **1**, **2**, and **4** which may justify this behaviour. It cannot be excluded, however, that the CD spectrum reported for $\text{Na}_3[\text{Fe}((S)\text{-BINOL})_3]$ is altered by the presence of a non-negligible amount of free BINOL, due to the partial decomposition of the complex [Peacock, R. D. and Siligardi, G., personal communications].

Table 5. Crystallographic Data for YbNa₃[(S)-BINOL]₃·6THF, 1

empirical formula	C ₈₄ H ₈₄ Na ₃ O ₁₂ Yb
formula weight	1527.52
temperature, K	298(2)
crystal system	hexagonal
space group	<i>P</i> 6 ₃ (no. 173)
<i>a</i> , Å	15.286(1)
<i>b</i> , Å	15.286(1)
<i>c</i> , Å	18.709(2)
α, deg	90
β, deg	90
γ, deg	120
volume, Å ³	3785.9(5)
<i>Z</i>	2
ρ _{calc} , mg/m ³	1.340
μ, mm ⁻¹	1.313
observed reflection [<i>I</i> > 2σ(<i>I</i>)]	1604
data/restraints/parameters	2459/1/276
<i>R</i> (<i>F</i> _o) ^a [<i>I</i> > 2σ(<i>I</i>)]	0.0395
<i>R</i> _w (<i>F</i> _o ²) ^a	0.0801

^a $R(F_o) = \frac{\sum ||F_o| - |F_c||}{\sum |F_o|}$; $R_w(F_o^2) = \frac{[\sum w(F_o^2 - F_c^2)^2]}{[\sum w(F_o^2)]^{1/2}}$; $w = 1/[\sigma^2(F_o^2) + (0.0427Q)^2]$, where $Q = [\text{MAX}(F_o^2, 0) + 2F_c^2]/3$.

ing fast and reliable information, which can be used to further investigate reaction intermediates.

Experimental Section

General Procedures, Instruments, and Materials. NMR spectra were recorded on a Varian VXR 300 spectrometer operating at 7 T, equipped with a VT unit stable within 0.1 °C. Where not otherwise specified, the temperature was 25 °C. Standard pulse sequences were used. All NMR spectra were recorded on samples dissolved in commercial *d*₈-THF stored over molecular sieves.

Absorption-NIR spectra were recorded at room temperature on a Perkin-Elmer Lambda 19 UV/vis/NIR spectrophotometer, under the following conditions: 7.5 nm/min, bandwidth 1.0 nm, NIR sensitivity 3, smooth bandwidth 2 nm. A square quartz cell was used, with a 1 cm path length. CD-NIR spectra were recorded on a JASCO 200 D spectropolarimeter, operating between 750 and 1350 nm, modified with a tandem Si/InGaAs detector with a dual photomultiplier amplifier. The bandwidth was 2.8 nm, and further narrowing of slit did not improve the resolution. The spectra were recorded at room temperature with 16 acquisitions at 50 nm/min with a 0.5 s time constant, and a 1 cm quartz cell was used. UV-absorption spectra were recorded using a UV-vis Varian CARY 4E spectrophotometer at room temperature using a cylindrical quartz cell with a 0.01 cm path length. CD-UV spectra were recorded on a JASCO J 600 spectropolarimeter, at room temperature under the following conditions: 10 nm/min, response 2 s, bandwidth 1.0 nm, in a cylindrical quartz cell with a 0.02 cm path length. All the spectra were recorded on samples dissolved in dry THF, obtained by distilling the commercial product (BAKER) under N₂, over Na-K alloy.

Commercial Yb(OTf)₃ was used (Fluka). LuCl₃ was purchased from ALFA. (*S*)-1,1'-bis(2-naphthol) was resolved from the commercial Fluka racemate according to the literature procedure.⁴⁰ *t*-BuONa was prepared by refluxing *t*-BuOH on Na for 3 days and removing *t*-BuOH excess. KHMDS (potassium bis(trimethylsilyl)azide) was used as the Aldrich toluene solution at 0.5 M.

Crystal Structure Determination. A colorless hexagonal prism of 1, of 0.33 × 0.24 × 0.20 mm³ dimensions, was sealed in a glass capillary and mounted on a Bruker P4 diffractometer, equipped with a graphite-monochromated Mo K_α radiation (λ = 0.710 73 Å). The cell parameters, calculated from the setting angles of 40 reflections having 7.54° < θ < 12.06°, are listed in Table 5, together with some other structural details. A total of 5672 intensities between 2.1° < θ < 25.0° was collected with the ω/2θ scan mode. Three standard reflections were measured every 97 measurements to check the sample decay and

equipment stability. The intensities were corrected for Lorentz and polarization effects and for absorption by means of a Gaussian method based on the crystal shape.⁴¹ The equivalent reflections were merged, leaving unmerged the Friedel pairs. 2459 *F*_o²'s, including the Friedel pairs, were then obtained (*R*_{int}, Σ|*F*_o² - *F*_o²(mean)|/Σ|*F*_o²| = 0.0502).

The structure solution was obtained in the space group *P*6₃ by the standard Patterson and Fourier methods. The refinements, based on full-matrix least-squares calculations on *F*², were done by means of the SHELX97 program.⁴² The H atoms were in part located in the difference Fourier map and in part placed in calculated positions. They were refined with the riding constraints. The absolute configuration was assumed to be correct on the basis of the Flack index -0.02(3).⁴³ The final refinement cycles gave the reliability factors listed in Table 5. The final difference Fourier map showed three peaks among 0.38 and 0.58 e⁻Å⁻³ at distances between 1.01 and 1.16 Å from the Yb atom. They are probably due to a defective description of its thermal motion and of absorption effects. The other residual electron-density peaks are lower than 0.3 e⁻Å⁻³, and none of them can be attributed to a water oxygen connected to ytterbium.

Synthesis of Na₃[Yb((S)-BINOL)₃] (1). To a stirred solution of (*S*)-1,1'-bis(2-naphthol) (258 mg, 0.9 mmol) in 8.0 mL of THF were added, in this order, a solution of Yb(OTf)₃ (186 mg, 0.3 mmol) in 3.0 mL of THF, *t*-BuONa (173 mg, 1.8 mmol), and a solution of 5.4 μL (0.3 mmol) of H₂O dissolved in 0.3 mL of THF, at room temperature and under argon atmosphere. After 1 h, the stirring was stopped and the clear yellow solution was separated by decantation. The volatile components were removed, the complex was dissolved in 1.9 mL of THF, and this solution was filtered over a 0.2 μm PTFE filter. *n*-Pentane (0.3 mL) was added dropwise to 0.6 mL of the solution, and the complex slowly crystallized over 1 day as pale yellow crystals. ¹H NMR (*d*₈-THF): δ 43.7 (br s, 6H, H-3), 14.5 (s, 6H, H-4), 7.4 (d, 6H, *J* = 8 Hz, H-5), 4.5 (m, 6H, H-6), 3.2 (m, 6H, H-7), -2.3 (d, 6H, *J* = 8 Hz, H-8). ¹³C NMR (*d*₈-THF): δ 149.4, 132.7, 125.1, 119.0, 118.2, 117.2.

Synthesis of K₃[Yb((S)-BINOL)₃] (2). To a stirred solution of (*S*)-1,1'-bis(2-naphthol) (258 mg, 0.9 mmol) in 8.0 mL of THF were added, in this order, a solution of Yb(OTf)₃ (186 mg, 0.3 mmol) in 3.0 mL of THF, KHMDS (3.6 mL, 1.8 mmol, 0.5 M in toluene), and a solution of 5.4 μL (0.3 mmol) of H₂O dissolved in 0.3 mL of THF, at room temperature and under argon atmosphere. After 1 h, the stirring was stopped and the clear yellow solution was separated by decantation. The volatile components were removed, the complex was dissolved in 1.9 mL of THF, and this solution was filtered over a 0.2 μm PTFE filter. *n*-Pentane (0.3 mL) of was added dropwise to 0.6 mL of the solution, and the complex slowly crystallized over 1 day as pale yellow crystals. ¹H NMR (*d*₈-THF): δ 20.5 (br s, 6H, H-3), 10.1 (s, 6H, H-4), 7.5 (d, 6H, H-5), 5.7 (m, 6H, H-6), 5.4 (m, 6H, H-7), 3.0 (d, 6H, H-8). ¹³C NMR (*d*₈-THF): δ 132.0, 129.0, 126.5, 122.1, 121.8, 119.6.

Synthesis of Na₃[Lu((S)-BINOL)₃] (4). To a stirred solution of (*S*)-1,1'-bis(2-naphthol) (143 mg, 0.5 mmol) in 1.8 mL of THF were added, in this order, a solution of dry LuCl₃ (70.3 mg, 0.25 mmol) in 2.8 mL of THF, *t*-BuONa (168 mg, 1.75 mmol), and a solution of 50 μL (2.8 mmol) of H₂O dissolved in 0.3 mL of THF, at room temperature and under argon atmosphere. The mixture was stirred for 20 h at 50 °C. The clear solution was separated by decantation. The volatile components were removed under vacuum (20 mmHg), the complex was dissolved in 1.9 mL of THF, and the solution was filtered over a 0.2 μm PTFE filter. *n*-Pentane (0.3 mL) was added dropwise to 0.6 mL of the solution, and the complex slowly crystallized over 1 day as colorless crystals. ¹H NMR (*d*₈-THF): δ 6.7 (m, 6H, H-8), 6.8 (m, 12H,

(40) Cai, D.; Hughes, D. L.; Verhoeven, T. R.; Reider, P. J. *Tetrahedron Lett.* **1995**, 36, 7991-7994.

(41) XSCANS, *X-ray Single-Crystal Analysis System*, rel. 2.1; Siemens Analytical X-ray Instruments Inc.: Madison, WI, 1996.

(42) Sheldrick, G. M. *SHELXTL-Plus*, relat. 5.1; Bruker Analytical X-ray Instruments Inc.: Madison, WI, 1997.

(43) Flack, H. D. *Acta Crystallogr.* **1983**, A39, 876-881.

H-6 and H-7), 7.6 (d, 6H, $J = 9$ Hz, H-4), 7.5 (d, 6H, $J = 9$ Hz, H-5), 7.4 (d, 6H, $J = 9$ Hz, H-3). ^{13}C NMR (d_8 -THF): δ 128.3, 128.3, 127.1, 125.9, 124.7, 120.2.

Acknowledgment. We thank CNR-ICCOM (Sezione di Pisa) and MIUR (National project "Stereoselezione in Sintesi Organica") for financial support.

Supporting Information Available: Cartesian coordinates of the optimized solution structure of **1**; EXSY spectrum of **2** in the presence of free BINOL (PDF, 4 pages); the X-ray crystallographic file (CIF format) for **1**. This material is available free of charge via the Internet at <http://pubs.acs.org>.

JA0297640